Article



The origin and impact of bound water around intrinsically disordered proteins

Korey M. Reid, 1,3 Abhishek K. Singh, 2,3 Chowdhury R. Bikash, 1 Jessica Wei, 1 Yftah Tal-Gan, 1 Nguyen Q. Vinh, 2,* and David M. Leitner^{1,7}

¹Department of Chemistry, University of Nevada, Reno, Nevada and ²Department of Physics and Center for Soft Matter and Biological Physics, Virginia Tech, Blacksburg, Virginia

ABSTRACT Proteins and water couple dynamically over a wide range of time scales. Motivated by their central role in protein function, protein-water dynamics and thermodynamics have been extensively studied for structured proteins, where correspondence to structural features has been made. However, properties controlling intrinsically disordered protein (IDP)-water dynamics are not yet known. We report results of megahertz-to-terahertz dielectric spectroscopy and molecular dynamics simulations of a group of IDPs with varying charge content along with structured proteins of similar size. Hydration water around IDPs is found to exhibit more heterogeneous rotational and translational dynamics compared with water around structured proteins of similar size, yielding on average more restricted dynamics around individual residues of IDPs, charged or neutral, compared with structured proteins. The on-average slower water dynamics is found to arise from excess tightly bound water in the first hydration layer, which is related to greater exposure to charged groups. The more tightly bound water to IDPs correlates with the smaller hydration shell found experimentally, and affects entropy associated with protein-water interactions, the contribution of which we estimate based on the dielectric measurements and simulations. Water-IDP dynamic coupling at terahertz frequencies is characterized by the dielectric measurements and simulations.

SIGNIFICANCE A combination of megahertz-to-terahertz dielectric spectroscopy and molecular dynamics simulations is carried out for the first time to probe the properties of the hydration water around intrinsically disordered proteins (IDPs), the nature and size of the hydration shell, and dynamic coupling between IDPs and water. The study finds greater heterogeneity in the rotational and translational dynamics of water around IDPs compared with structured proteins of similar size, yielding overall more restricted motion of water and an excess of tightly bound water molecules around the IDPs. These findings are used to estimate the entropy associated with IDP-water interactions. The dielectric spectra reveal dynamic coupling between water and IDPs at terahertz frequencies, which arises from greater backbone-water dynamic coupling compared with the structured proteins.

INTRODUCTION

Intrinsically disordered proteins (IDPs) and intrinsically disordered regions (IDRs) within otherwise structured proteins constitute a large fraction of the proteome of eukaryotes, contributing to cell function in a variety of ways, including transcription, signaling, and cell regulation (1-3). Lack of well-defined structure affects dynamic and thermodynamic properties of the proteins, which can facilitate bind-

Submitted October 23, 2021, and accepted for publication January 13,

https://doi.org/10.1016/j.bpj.2022.01.011

© 2022 Biophysical Society.

ing and allosteric regulation (4–6). However, a clearer picture of dynamic contributions to IDP function requires information about properties of hydration water and its interactions with IDPs, our understanding of which is still in its infancy. Hydration water dynamics and thermodynamics play central roles in the function of structured proteins (7), such as mediating structure, binding, and recognition (8-11). Structured protein-water coupling and interactions, and their contributions to function and folding, have long been the focus of attention (12–27), with studies pointing to the role of topography of protein surfaces controlling interactions with water (26–29). However, far less is known about the coupled dynamics of IDPs and water. Due to the inherent lack of structure of IDPs, the nature and origin of protein and hydration water dynamics will be different. To clarify the properties



³Korey M. Reid and Abhishek K. Singh contributed equally to this work.

^{*}Correspondence: vinh@vt.edu or dml@unr.edu

of hydration water around IDPs and coupled IDP-water dynamics, we present results of megahertz-to-terahertz dielectric spectroscopy measurements and molecular dynamics (MD) simulations of both solvated IDPs and structured proteins. The results of the experimental and computational study quantify for the first time the extent of the hydration shell around IDPs, the interaction between IDPs and water, and the origin of the excess tightly bound water to IDPs compared with structured proteins. The relatively large fraction of hydration water observed to be tightly bound to IDPs compared with the structured proteins affects the entropy associated with protein-water interactions, estimated in this work based on the experimental and simulation results.

Previous studies of IDP-water interactions and dynamic coupling indicate differences between water around IDPs compared with structured proteins. Water around IDPs, in most cases, has been observed to exhibit more sluggish dynamics compared with structured proteins, the origin of which has been attributed to several possible factors. Neutron scattering experiments reveal more restricted hydration water dynamics around IDPs (30), suggested to be due to constraints on the water molecules arising from a greater number of exposed side chains of IDPs compared with structured proteins. Time-resolved fluorescence measurements have also indicated more restricted dynamics of water around IDPs compared with structured proteins near fluorescent labels (31,32). Computational studies have quantified some of the differences between water dynamics around IDPs and structured proteins, indicating that water molecules may be less mobile around IDPs compared with structured proteins (33,34), although the opposite trend was inferred based on the results of one study (35). More restricted hydration water dynamics around IDPs found in computational work was suggested to be due to the greater number of exposed charged groups (33), as water near charged groups may be less mobile. Heterogeneity of water dynamics over different domains of an IDP has been observed in time-dependent Stokes shift measurements at several specific sites spanning three domains, and by companion MD simulations (31,36). These findings are further supported by recent time-resolved Stokes shift measurements of IDP complexes (32). However, the extent of the hydration shells around IDPs, which may provide significant insight into these observations, remains unknown.

Overall, based on the previous work, a picture has emerged where water in the first hydration layer usually exhibits more restricted dynamics around IDPs, which may be attributed to greater contact, due to a larger solvent accessible surface area, between residues and water (30,31), as well as to the greater number of exposed charged groups compared with structured proteins (33), since water around charged groups appears less mobile than around neutral groups. A comprehensive view of all these aspects is provided here. Based on our experimental and simulation results, we show that both factors, the greater number of exposed charged groups of IDPs and greater contact with water, are responsible for the observed sluggish motion of water around IDPs and are related.

The broadband dielectric measurements provide detailed information about water throughout the hydration shell, and not only near a specific fluorophore as in many previous experiments on IDP-water interactions to date, allowing for a classification of the hydration layers that are relatively tightly and less tightly bound to the IDP. We find the excess tightly bound water around IDPs to be commensurate with the greater water density found in the first hydration shell around the IDPs in the MD simulations. The additional tightly bound water corresponds to an entropy that is about 1.8 cal/(mol-ofresidue • K) lower. The dielectric spectra also reveal smaller hydration shells around the IDPs, containing less loosely bound water than around the structured proteins. This result is consistent with the larger number of more tightly bound water molecules in the first layer, in harmony with early pictures of biological water surrounding proteins (37,38), as we discuss here. The dielectric measurements and results of the MD simulations also reveal the collective vibrational modes of the IDP dynamically coupled to water in the THz region.

Dynamic, spectroscopic, and thermodynamic properties of five systems are studied here, including three IDPs and two structured proteins. All the IDPs are IDRs from natural proteins and contain 22 to 26 residues. In this size range, all residues are in contact with water, so we do not need to differentiate between core and surface residues. The IDPs, which contain different numbers and types of charged groups, are IDRs from three independent systems. These systems include a disordered domain of chicken fibrinogen, a disordered strand of a stannin, and another one from the C-terminal end of non-muscle myocin II, which we refer to as D-fibringen (DF), D-stannin (DS), and D-myocin (DM), respectively. Both experimental and computational circular dichroism (CD) spectra indicate that the IDRs remain disordered as the IDPs of this study. The two structured systems include a wild-type protein (HP24wt) and a mutant, HP24stab, which were selected because of their similar size to the IDPs. The 24-residue HP24wt is partially unstructured, unlike its native form found in the larger headpiece domain, containing floppy N and C termini, while maintaining α helical content in the central region (39). HP24stab contains two point mutations that stabilize the structure, resulting in full recovery of the helical content found natively (39). The sequences of all systems are listed in Table 1.

MATERIALS AND METHODS

Synthesis

The synthetic methods and characterization of each of the synthesized peptides can be found in the supporting material. Further characterization by CD spectroscopy was carried out on all the systems. Details concerning the experimental CD measurements and the method used to compute the

TABLE 1 Peptide labels, single letter code primary sequence, and sequence length

System	Sequence	Length	N^+	N ⁻	N ^{TOT}
DF	QDGKTTFEKEGGGGRGPRILENMHES	26	4	5	9
DS	LRLQRISQS <i>EDEE</i> SIVG D GETKE	23	3	7	10
DM	RNRLRRGPLTFTTRTVRQVFRL	22	7	0	7
HP24wt	MTRSAFANLPLWKQQNLKK <i>E</i> KGLF	24	5	1	6
HP24stab	MTRSAFANLPLWKQQALMKEKGLF	24	4	1	5

Positively charged residues are underlined, while negatively charged residues are bold and in italics.

CD spectra are provided in the supporting material, and the corresponding spectra for each system appear in Fig. S2.

Computational

Each peptide listed in Table 1 was constructed using PyMOL 2.1.0, with both ends capped by an acetyl protecting group and N-methyl amide for the N terminus and C terminus, respectively. Each linear structure was minimized under the MMFF94s forcefield from the PyMOL optimize function. For comparison, villin headpiece subdomain, HP24wt (PDB: 4ZC3), and a mutant variant, HP24stab (PDB: 4ZC4), were included as controls because one is partially structured and the other fully structured, respectively. Simulations on the systems were carried out with GROMACS 2016.6 and 2019.6 employing the CHARMM 36m forcefield including optimized parameters for the study of both structured and unstructured proteins (40). All systems were solvated in a dodecahedron TIP3P water box, with minimum distance from the protein to the edge of the box of 1.4 nm. We have found alternative water models, specifically SPC/E, used in past computational studies to model properties underlying dielectric spectra of solvated biomolecules (41,42), to sometimes generate structure in IDPs, while TIP3P preserves the disorder. The systems were neutralized by adding Na⁺ and Cl⁻ ions, bringing the final concentration to 0.15 M. From the MD simulation data, structural properties were determined. CD spectra were computed using SESCA (43) for comparison with experimentally acquired spectra. Clusters of similar structures for each system were computed using the GROMACS geometric clustering algorithm. Cluster membership was determined with a neighbor RMSD cutoff of 0.22 nm for all IDPs and HP24wt, and 0.12 nm for HP24stab, where all structures belonging to a cluster are within the cutoff of a central structure and all structures uniquely belong to a cluster. A smaller value was taken for HP24stab to emphasize the greater similarity in structure; the selection of 0.22 nm for HP24stab resulted in a single geometric cluster.

Water properties were determined by the simulation data, including the radial distribution function, hydrogen bond time correlation function, and the vibrational density of states (VDOS). The first-order rotational time correlation functions of the water dipole were calculated as

$$C_1(t) = \langle P_1(\widehat{\mu}(t) \cdot \widehat{\mu}(0)) \rangle,$$
 (1)

where $P_1(x)$ is the first-order Legendre polynomial, the individual time correlations for each water are averaged over time, and $\widehat{\mu}(t)$ is the unit vector along the dipole moment vector at time, t. The hydrogen bond correlation function, $C_{HB}(t)$, the probability that a hydrogen bond at an initial time is found at a later time, t, was calculated for residue-water hydrogen bonds and for water-water hydrogen bonds, where standard distance and angle criteria were applied. Specifically,

$$C_{HB}(t) = \frac{\langle h_i(t) \cdot h_i(0) \rangle}{\langle h_i(0) \rangle}, \tag{2}$$

where, $h_i(t)$ is a Boolean function describing the existence of the ith hydrogen bond at time, t, that existed at the initial t = 0, whether or not it broke at intermediate times. A hydrogen bond between a donor, D, and acceptor, A, D-H... A, is formed when the distance between A and D is within 3.5 Å and the DHA angle is greater than or equal to 150°. $C_{\rm HB}(t)$ was also computed separately for individual residue-water contacts of each system. The number of water molecules that interact with a residue was compared with the lifetimes, where that number is defined as any atom of a water molecule within 3.5 Å of any atom of a residue.

Experimental

The dielectric spectroscopy measurements were performed on 8.3 mM DF, 9.1 mM HP24wt, and 8.7 mM HP24stab solutions. We measured the complex dielectric response of the solutions using a broadband dielectric spectrometer from 100 MHz to 1.12 THz (0.000334-37.36 cm⁻¹). The spectrometer consists of a commercial Vector Network Analyzer (VNA) from Agilent (N5225A PNA), which covers the frequency range from 10 MHz to 50 GHz, and frequency extenders. Frequency extenders from Virginia Diodes (Charlottesville, VA) are interfaced with the VNA to generate continuous waves at terahertz frequencies. Seven different waveguide rectangular (WR) modules are used to cover a frequency region from 55 GHz to 1.12 THz. The system enables us to measure simultaneously the absorption coefficients and refractive index (i.e., the dielectric dispersion and loss) of aqueous peptide solutions. All measurements were performed using a variable-path-length sample cell at 25°C, controlled with an accuracy of ± 0.02 °C. An ultra-precision linear stage from Newport (XMS50) is used to control and measure the path length of the solutions in the sample cell with nanometer precision (41,42,44-47). Additional details of instrumentation and data processing appear in the supporting material.

The absorption coefficient, $\alpha(\nu)$, the refractive index, $n(\nu)$, and the complex dielectric response of pure water, 8.3 mM DF, 9.1 mM HP24wt, and 8.7 mM HP24stab solutions were measured (supporting material, Fig. S6). The main dielectric loss peak has been observed at 19.25 GHz (i.e., 8.27 ps) for pure water and all peptide solutions is a relaxation mode of bulk water (47-49). In the megahertz to gigahertz frequency region, emergence of the dielectric response due to the relaxation of water molecules having direct or indirect contacts with protein surface appears, corresponding to dynamics slower than bulk water dynamics. The distinct contribution to the hydration dynamics can be identified by analyzing the complex dielectric function, $\varepsilon^*(\nu)$, using a Debye model composed of three individual Debye relaxation modes corresponding to orientational relaxation of water molecules in the solutions.

The complex dielectric response, $\varepsilon_{\rm sol}^*(\nu)$, of the solutions can be calculated from the absorption coefficient and refractive index as a function of frequency, ν , in the form (50),

$$\varepsilon_{\text{sol}}^*(\nu) = \varepsilon_{\text{sol}}'(\nu) + i\varepsilon_{\text{sol}}''(\nu)$$
 (3)

$$\varepsilon'_{\text{sol}}(\nu) = n^2(\nu) - \left(c\alpha(\nu)/(4\pi\nu)\right)^2 \tag{4}$$

$$\varepsilon_{\text{sol}}''(\nu) = 2n(\nu)c\alpha(\nu)/(4\pi\nu) - \sigma/(2\pi\nu\varepsilon_0)$$
 (5)

where $\varepsilon'_{sol}(\nu)$ and $\varepsilon''_{sol}(\nu)$ are real and imaginary parts (or the dielectric dispersion and loss), respectively, of the complex dielectric response, ε_0

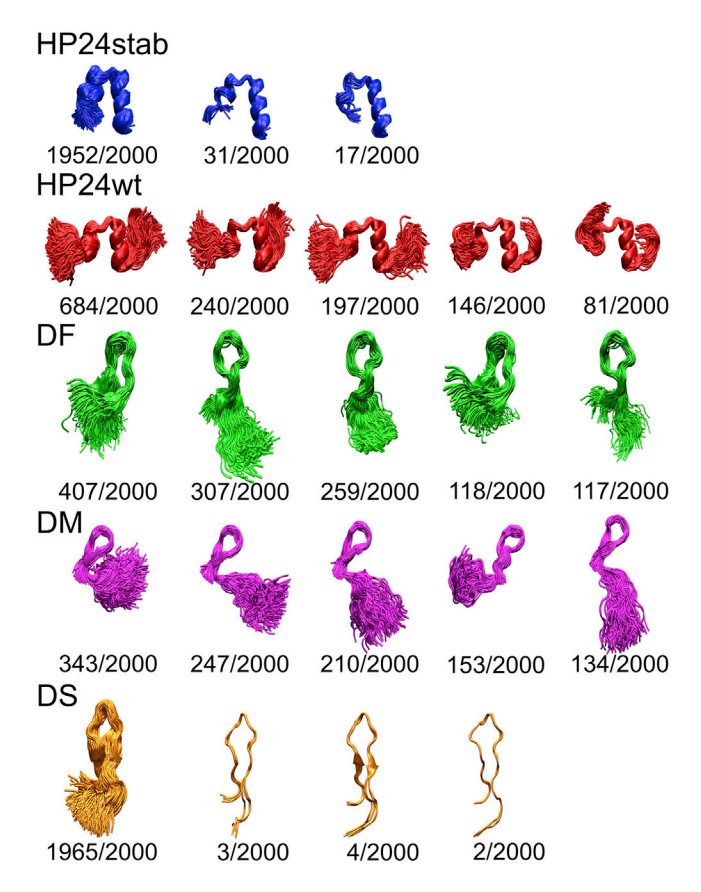


FIGURE 1 Structures and frequency of occurrence of HP24stab, HP24wt, DF, DM, and DW are indicated. The five largest clusters of configurations with the greatest number of participants are shown. Clusters were constructed from a total of 2000 structures equidistant in time. Configurations have been clustered as described in the text. To see this figure in color, go online.

is the permittivity of the vacuum, σ is the electrical conductivity of the solution, and c is the speed of light.

The distinct contributions to the hydration dynamics can be identified by analyzing the complex dielectric function, $\varepsilon^*(\nu)$, using a Debye model composed of three individual Debye relaxation modes, capturing contributions from tightly bound, loosely bound, and bulk water, respectively, in the solutions. Such a model has often been used to characterize hydration dynamics in the form (41,42,45-47),

$$\varepsilon_{\text{sol}}^{*}(\nu) = \varepsilon_{\text{sol}}'(\nu) + i\varepsilon_{\text{sol}}''(\nu) = \varepsilon_{\infty} + \frac{\varepsilon_{S} - \varepsilon_{1}}{1 + i\omega\tau_{1}} + \frac{\varepsilon_{1} - \varepsilon_{2}}{1 + i\omega\tau_{2}} + \frac{\varepsilon_{2} - \varepsilon_{\infty}}{1 + i\omega\tau_{D}},$$
(6)

where $\Delta \varepsilon_1 = \varepsilon_S - \varepsilon_1$, $\Delta \varepsilon_2 = \varepsilon_1 - \varepsilon_2$, and $\Delta \varepsilon_D = \varepsilon_2 - \varepsilon_\infty$ represent the dielectric contributions of individual relaxation processes to the total dielectric response from the tightly bound, loosely bound, and bulk water, respectively. ε_S is the static permittivity given by $\varepsilon_S = \varepsilon_\infty + \sum_{i=1}^3 \Delta \varepsilon_i$, and $arepsilon_{\infty}$ includes contributions to the dielectric response from all polarization modes at frequencies much higher than the probed range. $\omega = 2\pi\nu$ is the angular frequency of the applied electric field. τ_1 corresponds to the orientational relaxation dynamics of tightly bound water molecules, which directly interact with the protein surface. Since these water molecules are under direct influence of electrostatic fields of proteins, they possess the least orientational freedom of all the bound water molecules. τ_2 corresponds to the relaxation time of water molecules in the outer hydration shells that are weakly influenced by the presence of proteins. The fast relaxation time, $\tau_{\rm D}$, represents the orientational relaxation of bulk water, corresponding to the rearrangement of the hydrogen bond network in bulk water.

RESULTS AND DISCUSSION

We begin with evaluation of structures of the five systems. This information is illustrated by clustering of the MD simulation structural data, following the clustering methodology discussed in the previous section. Groups of structures and frequency of occurrence are plotted in Fig. 1. The relatively rigid HP24stab displays two α helical domains separated by a rigid turn, with one cluster containing 98% of structures and two others similar to the dominant one. The structures sampled by HP24wt indicate the center is dominated by an α helical region. The conformational ensembles found for the IDPs vary from system to system. DS exhibits a variety of extended structures, similar to the form of the disordered region of human stannin, an extended horseshoe conformation (51). DM and DF are characterized by a greater diversity in the conformational ensemble as seen by the emergence of many clusters, which may facilitate binding and recognition (52,53). Additional structural information is provided by CD spectra, both experimental and spectra computed with the simulation data, which are plotted in Fig. S2. The CD spectra confirm the helical structure of HP24stab, some structure for HP24wt, and lack of structure of the IDPs (DF, DS, and DM), consistent with the features illustrated in Fig. 1.

We turn now to dynamics of the hydration water captured both by the dielectric spectra and MD simulations. We will consider rotational and translational dynamics of hydration water before addressing the size of the hydration layer and coupled IDP-water dynamics. The rotational relaxation dynamics illustrates well differences between motion of water around IDPs and structured proteins. Rotational dynamics of water is captured in the dielectric loss spectra and the rotational time correlation function for hydration water, which we plot in Fig. 2 for DF, HP24wt, and HP24stab. The dielectric loss spectra for the hydration water around these systems, plotted in Fig. 2 A, are determined from the dielectric spectra for DF, HP24wt, and HP24stab solutions (Fig. S6), as explained in the previous section. We plot in Fig. 2 B the rotational time correlation function, $C_1(t)$, for water molecules in the hydration layers, obtained with Eq. 1 using the MD simulation data for these systems.

A clear distinction is observed in both panels of Fig. 2 for the rotational relaxation dynamics of water in the hydration layers around DF compared with that in the hydration layers around the more structured HP24stab and HP24wt. The peak in the dielectric loss spectrum for DF lies around 1 GHz, compared with ≈ 3 GHz for HP24stab and HP24wt. Similarly, the results of the MD simulations indicate a striking difference between the rotational relaxation of water

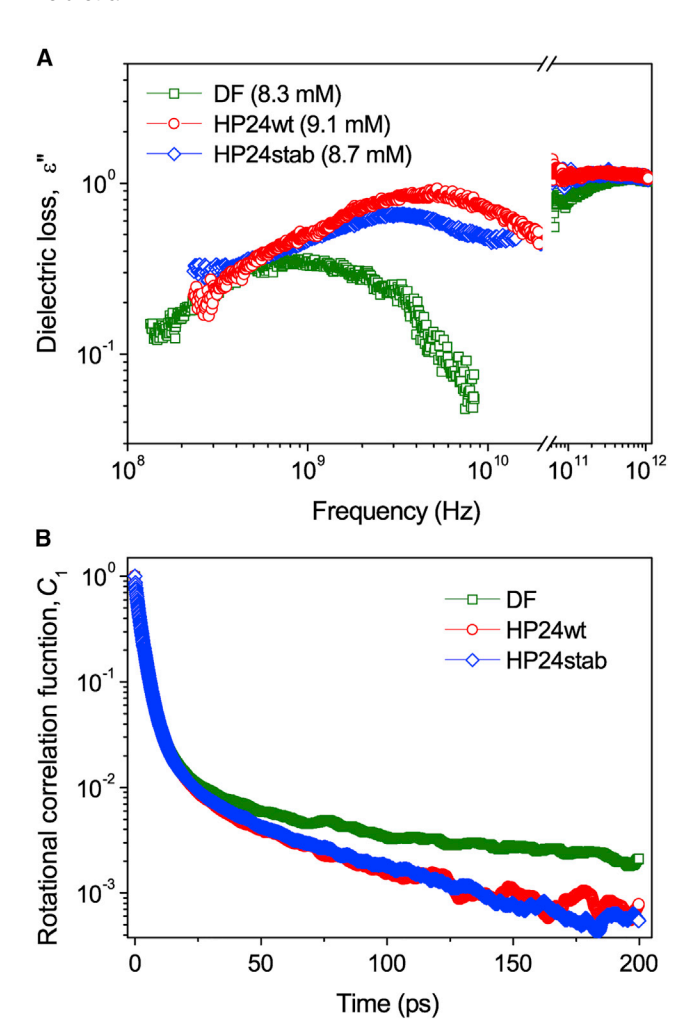


FIGURE 2 Rotational relaxation of water molecules around two structured and one disordered system obtained from experiment and from molecular simulations is plotted. (A) Measured dielectric loss spectra for DF (green), HP24wt (red), and HP24stab (blue). (B) Computed rotational time correlation function, $C_1(t)$, plotted for DF (green), HP24wt (red), HP24stab (blue). To see this figure in color, go online.

molecules in the hydration layers around DF and around HP24stab and HP24wt. Water molecules around the latter two relax at about the same rate, whereas they relax about 70% more slowly around DF.

We will return to rotational relaxation of water around the IDPs and structured proteins, but first examine other relaxation processes to illustrate the generally more restricted dynamics of water around IDPs and to examine the origin. Several computational studies of hydration water dynamics around IDPs have addressed the lifetimes of hydrogen bonds between water and IDPs. We therefore consider this property and look closely at the role of different classes of residues toward the dynamics. The hydrogen bond lifetime is determined from the hydrogen bond correlation function, $C_{\rm HB}(t)$, for hydrogen bonds between water molecules and residues. The results obtained for the five systems of this study with Eq. 2 using the results of the MD simulations are plotted in Fig. 3 A. We observe that the hydrogen bonds rearrange more slowly around each of the IDPs than around the more structured HP24stab and HP24wt. The hydrogen bond lifetimes, obtained as the time to decay to e^{-1} , for DF, DS, and DM are 12.6, 13.1, and 11.2 ps, respectively, while for HP24wt and HP24stab they are 9.94 ps and 9.53 ps, respectively. We note that the relatively short average lifetime for DM compared with the other IDPs may be due to its more compact structure compared with the other IDPs (Fig. 1).

We note that a similar trend is found for other measures related to the translational dynamics of water molecules in the hydration layers around these systems, such as the survival time correlation function, S(t), which quantifies the probability that water molecules in a hydration layer at time 0 are still found there at a later time, t. Results for S(t), plotted in Fig. S4 for the first two hydration layers, again indicate more restricted motion of water molecules around the IDPs than around HP24. For example, the survival time, determined as the time for S(t) to decay to e^{-1} , for a water molecule in the first layer is 43.8 ps, 41.9 ps, and 41.4 ps, for DF, DS, and DM, respectively, and is 38.3 ps and 37.2 ps for HP24wt and HP24stab, respectively.

We now examine $C_{HB}(t)$ more closely to consider possible origins of the more restricted dynamics of water around IDPs compared with structured proteins. In Fig. 3, we plot lifetimes computed for hydrogen bonds between water and individual residues of each system. Plots of all $C_{\rm HB}(t)$, from which the hydrogen bond lifetimes are obtained as the value where $C_{HB}(t)$ reaches e^{-1} , appear in Fig. S3. In Fig. 3 B-F, the average hydrogen lifetime between water molecules and each residue is indicated by a separate point, and the residues are indicated as positively charged, negatively charged, and neutral.

We also list the contributions of residues that are positively charged, negatively charged, and neutral to the average lifetimes in Table 2. There we see that the lifetimes of hydrogen bonds between water and negatively charged groups are typically longer than around positively charged groups, which are in turn somewhat longer on average than lifetimes for neutral groups. The negatively charged groups can interact with two hydrogens of a water molecule and thereby restrict dynamics more than a positively charged group.

In addition to hydrogen bond lifetimes, we also plot in Fig. 3 B-F for each residue of each system the number of water molecules within 3.5 Å of any atom of the residue, which we take as a measure of the number of nearby water molecules. There is a clear correlation between the number of water molecules close to a residue and whether or not the residue contains charged groups. With few exceptions, more than 20 water molecules are in the vicinity of residues with charged groups, whereas fewer than 20 water molecules are near residues that lack charged groups. For neutral groups, the number of nearby water molecules is between 10.1

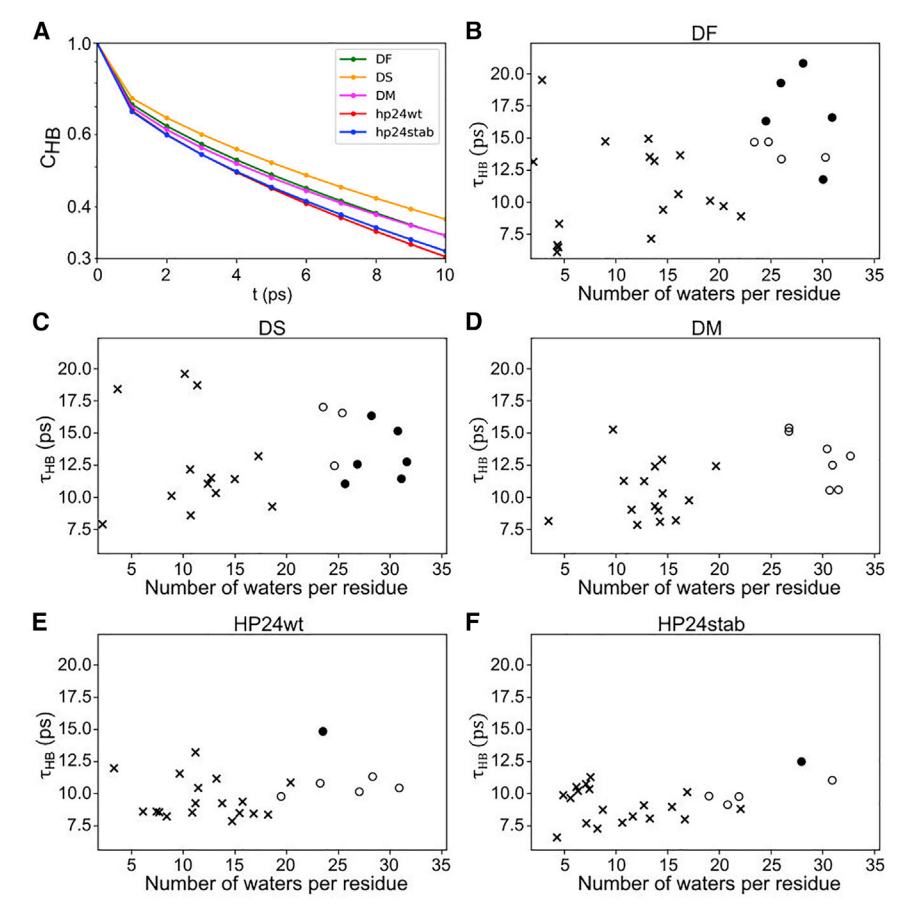


FIGURE 3 Lifetimes of hydrogen bonds between water molecules and residues obtained from molecular simulations and number of water molecules near each residue are plotted for three disordered and two structured systems. (A) Correlation function for hydrogen bonds, $C_{HB}(t)$, between water molecules and DF, DS, DM, HP24wt, and HP24stab (log-linear plot). $C_{HB}(t)$ is the probability that a hydrogen bond identified during a simulation is found intact at a later time, t. Lifetimes of hydrogen bonds between water and individual residues and the corresponding mean number of water molecules in the vicinity of a residue (see text for criterion of vicinity) are plotted in (B) DF, (C) DS, (D) DM, (E) HP24wt, and (F) HP24stab. Each point in (B-F) corresponds to one of the residues of the system, and all residues of each system are indicated, characterized as anionic (filled circles), cationic (open circles), and uncharged (x). To see this figure in color, go online.

and 13.2 for the five systems. For the charged groups the range is 23.2–30.0. Adding more charged groups to a system increases the number of nearby water molecules, and, on average, there are more water molecules near each residue of the IDPs than the structured proteins. For DF, DS, and DM, there are on average 16.8, 18.1, and 18.6 water molecules near each residue, respectively. For HP24wt, there are 15.4 water molecules on average near each residue, and for HP24stab there are 13.0.

These values depend on the chemical groups in contact with water and not merely the solvent accessible surface area (SASA). We calculated SASA values to be 32.1, 26.5, 31.5, 30.3, and 24.5 nm² for DF, DS, DM, HP24wt, and HP24stab, respectively. Accounting for system size, we find that the SASA of HP24wt is larger per residue than all but DM. We thus find the restricted dynamics of water around IDPs to arise from the greater density of nearby water molecules compared with structured proteins of similar size, due in large part to the greater number of charged groups of the IDPs.

As noted above, it has been suggested in earlier work that hydration water around IDPs is less mobile than around structured proteins, because water molecules are less mobile near charged groups and there are typically more exposed charged groups on IDPs than structured proteins. The number of charged groups is indeed larger for the IDPs than for HP24 (Table 1), and the relative lifetimes of the hydrogen bonds between water and each of the five systems correlate with the relative number of charged groups for each system. However, the longer lifetimes of hydrogen bonds between water molecules and charged groups does not fully explain the longer average hydrogen bond lifetime between water molecules and an IDP. We find the hydrogen bond lifetime is on average longer around charged groups and neutral groups of the IDPs than around the respective groups of the structured proteins. In fact, the lifetime is longer on average for hydrogen bonds between water and the neutral groups of the IDPs than the overall average hydrogen bond lifetime between water and the structured proteins. Indeed, lifetimes around neutral groups of some of the IDPs are longer than lifetimes around some of the charged groups of the structured proteins. As apparent in Fig. 3 and from the data listed in Table 2, the variation in lifetimes is greater for the IDPs than the structured proteins. The shortest lifetimes observed are comparable for all systems, but the longest are considerably greater for the IDPs than the structured proteins, regardless of whether the residue is charged or not. As a result, the lifetimes for IDPs are shifted to larger values for hydrogen bonds between water molecules and any class of residue.

TABLE 2 Hydrogen bond lifetimes (in picoseconds) around neutral and charged groups for each system

System	DF	DS	DM	HP24wt	HP24stab
Neutral	11.0 ± 3.6	12.5 ± 1.5	10.4 ± 2.1	9.53 ± 1.5	9.31 ± 1.5
Positive charge	14.0 ± 0.6	15.3 ± 2.0	13.0 ± 1.8	10.4 ± 0.5	9.77 ± 0.8
Negative charge	17.1 ± 3.1	15.1 ± 5.4	_	14.8	12.5

The number of positively and negatively charged residues is listed in Table 1. If there is no residue in a category, we report no time, and if there is more than one residue, we report an average value \pm one standard deviation.

The charged groups influence the number of nearby water molecules, as seen in the results plotted in Fig. 3, leading to a larger number of water molecules in the first hydration shell, which are around both the charged and neutral groups of the protein. That is also seen upon calculation of the number of water molecules in the first few hydration shells around each of the systems, listed in Table 3, where the average total number of water molecules within 3, 5, and 8 Å of the surface of each system appears. Per residue, the average number of water molecules in the first hydration layer around DF, DS, and DM is 8.0, 8.0, and 9.6, respectively, compared with 7.5 and 6.5, respectively, for HP24wt and HP24stab. The enhancement of water in the first hydration shell around the IDPs is consistent with a greater number of water molecules tightly bound to the systems determined by the dielectric spectra, which we turn to

Broadband dielectric spectroscopy from megahertz to terahertz frequencies probes the dynamics as well as the number of water molecules in the hydration layers. In view of the heterogeneous nature of orientational dynamics of water molecules around a protein surface, it is both convenient and consistent with the data to classify water molecules in the hydration layer as tightly bound (TB) and loosely bound (LB) water. The dielectric spectra (Fig. S6) collected from the spectrometer for DF, HP24wt, and HP24stab solutions have been deconvoluted into three Debye components, assigned to contributions from TB, LB, and bulk water orientational dynamics, which are plotted in Fig. 4 A-C. To identify the dielectric response from hydration water, the contribution of bulk water to the total dielectric response characterized by the relaxation time, τ_D , and the dielectric strength, $\Delta \varepsilon_{\rm D}$, is subtracted from the measured dielectric spectrum (Fig. 4 D–F). After the subtraction, the complex dielectric spectra, shown in Fig. 4 D-F, indicate contributions to the dielectric response from hydration water molecules.

The size of the hydration layers, including the contributions from TB and LB water, can be determined from the dielectric strength of bulk water in the solutions, which contributes to the main dielectric loss at 19.25 GHz. The peak value of the dielectric loss and the dielectric strength of bulk water (Table 4) in protein solutions are lower compared with pure water. This observation is consistent with earlier reports (42,54,55) and can be attributed to the presence of proteins in solution and the hydration effect. Proteins have very low absorption at the megahertz to gigahertz frequencies, in contrast to pure water. When proteins are dissolved, they replace water molecules, and as a result the total absorbance decreases in this spectral region. In addition, a large fraction of water molecules is kinetically retarded due to protein-water interactions. An estimate for the total number of water molecules in the hydration layers, the hydration number, N_{hyd} , is given by (41,42,54)

$$N_{\text{hyd}} = \frac{c_{\text{w}} - \frac{\Delta e_{\text{w}}}{\Delta e_{\text{pure}}} c_{\text{pure}}}{c}, \tag{7}$$

where c and $c_{\rm w}$ are the molar concentrations of protein and water, respectively, in the solution, $c_{\text{pure}} = 55.35 \text{ M}$ is the molarity of pure water, $\Delta \varepsilon_{\text{pure}} = 73.25$ is its dielectric strength at 25°C, and $\Delta \varepsilon_{\rm w}$ is the dielectric strength of bulk water in the aqueous solution. The hydration number estimated with Eq. 7 is 200 \pm 25, 218 \pm 25, and 272 \pm 30 for DF, HP24wt, and HP24stab solutions, respectively (Table 4).

The dielectric strengths and relaxation times obtained from fitting the dielectric spectra to Eq. 6 are provided in Table 4 for the protein solutions. There are differences in the relative number of hydration water molecules that can be characterized as TB and LB. In HP24wt and HP24stab solutions, the dielectric strength of LB water is ≈ 4.5 and ≈ 3.1 times that of TB water, respectively, indicating a large fraction of LB water and a hydration structure that extends over several hydration layers from the protein surface, which can also be seen by comparing the number of hydration water molecules with the hydration layer size for each solute, listed in Table 4. Such extended hydration layers are found for many structured proteins (12,56). For the IDP solution, the dielectric strengths of LB and TB water are comparable in magnitude, indicating a smaller hydration shell. This is consistent with earlier studies indicating mutation and structural destabilization can reduce the size of the hydration layer (57).

The rotational relaxation dynamics of water molecules around the IDP and structured proteins is different. The time constants for TB water are about 300 ps for each system (Table 4). For LB water molecules, we obtain $131 \pm 10 \,\mathrm{ps}$, 32 \pm 5 ps, and 45 \pm 5 ps for DF, HP24wt, and HP24stab, respectively. While the relaxation times for the LB water around the two structured proteins are similar, the relaxation time for water around the IDP is about three to four times longer. Since these times are connected to rotational relaxation times of water molecules around the proteins, we have

TABLE 3 Average number of water molecules together \pm 1 standard deviation computed to be within 3, 5, and 8 Å of the peptide surface for each system

System	DF	DS	DM	HP24wt	HP24stab
3A	206 ± 8	181 ± 9	212 ± 10	180 ± 8	156 ± 8
5A	444 ± 14	438 ± 18	474 ± 17	410 ± 13	352 ± 12
8A	$941~\pm~26$	$922~\pm~34$	$997~\pm~33$	$890~\pm~28$	$757~\pm~20$

computed the first-order rotational time correlation function, $C_1(t)$, of hydration water molecules around the two HP24 proteins and the three IDPs. The results for water molecules within the first hydration layer of DF, HP24wt, and HP24stab are shown in Fig. 2, and for all systems in the first three hydration layers in Fig. S5. All the results were fitted to a multi-exponential function. The slow relaxation times are 59.9 \pm 0.3 ps, 71.5 \pm 0.6 ps, 108.9 \pm 1.0 ps, 86.9 \pm 0.6 ps, and 91.2 \pm 0.1 ps, respectively, for HP24stab, HP24wt, DF, DS, and DM. Notably, the time constants for the water around the IDPs are all longer than those around the structured proteins; for DF, it is about 70% larger. Overall, these results are consistent with the disparity in dielectric relaxation time observed for the water molecules around DF compared with HP24.

The dynamics at the terahertz frequencies involves largescale motions of proteins strongly coupled to water, where TB water molecules interact strongly with the protein surface forming hydrated proteins (45,55). In the context of the dielectric spectroscopy, the complex dielectric response of the protein solution, $\varepsilon_{\mathrm{sol}}^*$, results from the combination of the dielectric response of hydrated proteins and water. The wavelengths of the probing electromagnetic waves are orders of magnitude larger than the size of hydrated proteins, thus each protein solution can be approximated as an effectively homogeneous medium. Several dielectric models based on the effective-medium approximation (EMA) have been proposed (58-61). The Bruggeman model is well suited for aqueous protein solutions (58,59), and works well for a large range of protein concentration as well as for systems with high dielectric contrast between individual components. The Bruggeman model yields

$$f_{\rm hp} \frac{\varepsilon_{\rm hp}^* - \varepsilon_{\rm sol}^*}{\varepsilon_{\rm hp}^* + 2\varepsilon_{\rm sol}^*} + \left(1 - f_{\rm hp}\right) \frac{\varepsilon_{\rm wat}^* - \varepsilon_{\rm sol}^*}{\varepsilon_{\rm wat}^* + 2\varepsilon_{\rm sol}^*} = 0, \qquad (8)$$

where $\varepsilon_{\rm hp}^*$ and $\varepsilon_{\rm wat}^*$ are the complex dielectric response of hydrated proteins and pure water, and $f_{\rm hp}$ is the volumetric fraction of hydrated proteins in solution. In this approach, we assume that the TB water, with relaxation times $\sim\!300$ ps, about 1000 times slower than the typical timescale of collective motions, and the protein essentially form a single entity. The proteins are approximated as spherical macromolecules with an average radius, $R_{\rm P}$. Thus, the volumetric fraction of hydrated protein is $f_{hp} = (N_P/V)(4\pi/3)(R_P+d)^3$, where $N_{\rm P}$ is number of protein molecules, d is the thickness of the TB water, and $N_{\rm P}/V$ is the concentration of protein in solution.

Employing the Bruggeman EMA, we have extracted the complex dielectric responses for the hydrated proteins, plotted for the three systems in Fig. 5. With this analysis we obtain 90 ± 10 , 73 ± 8 and 65 ± 8 TB water molecules for DF, HP24wt, and HP24stab, respectively (Table 4). Using the hydration layer sizes reported above, the number of TB water molecules is about one-third to one-fourth the number of LB water molecules around HP24 and HP24stab. For the IDP, the number of TB water is approximately equal to the number of LB water. These estimates are similar to those obtained from the dielectric strengths discussed above.

While we find on average more TB water in the hydration layer around IDPs, and we also find fewer LB water molecules and overall a smaller hydration shell compared with the structured proteins. This finding is consistent with an early picture of biological water (37,38), in which many water molecules in contact with the biomolecule are relatively TB, exchanging with water in the immediate surroundings, the LB water discussed here, which in turn exchange with bulk water. We have seen here that a larger number of water molecules around IDPs is TB than around structured proteins, leading to slower exchange with water in the immediate surroundings and a smaller fraction of LB water. The dielectric spectra indicate relaxation times about three times slower for the IDP than the structured proteins and a ratio of TB to LB water that is about three times greater for the IDP than the structured proteins. These values are consistent with an equilibrium model for the exchange of water molecules between these layers (37), where the ratio of the rate constants for the formation of TB from LB water to the formation of LB from TB water corresponds to the ratio of the number of TB to LB water molecules.

The number of water molecules TB to the protein surface sheds light on the thermodynamic properties associated with protein-water interactions for IDPs and structured proteins. The 90 TB water molecules around DF can be compared with the on-average 69 TB water molecules around the structured HP24. The former represents 3.5 TB water molecules per residue compared with 2.9 TB water molecules per residue for HP24; i.e., a difference of 0.6 TB water molecules per residue of DF compared with HP24. This value compares well with the number of excess water molecules computed for the first hydration layer of DF compared with HP24 (Table 4), which is 0.9 water molecules per residue larger. Based on the entropy difference for the release of one water molecule from a tight protein-water interaction, about 3 cal/(mol-of-residue • K) (62), we estimate, using a difference of 0.6 TB water molecules per residue, that the entropy of the water in the hydration layer around DF is lower than that around the HP24 by 1.8 cal/(mol-of-residue • K), or about 500 cal/(mol-of-residue) contribution to the free energy difference at 300 K.

This contribution can, at least in part, offset the entropic cost of binding of ligands to IDPs and IDRs, including the entropic cost of structure formation that sometimes accompanies IDP-ligand binding (4,32,63,64), as only small shifts

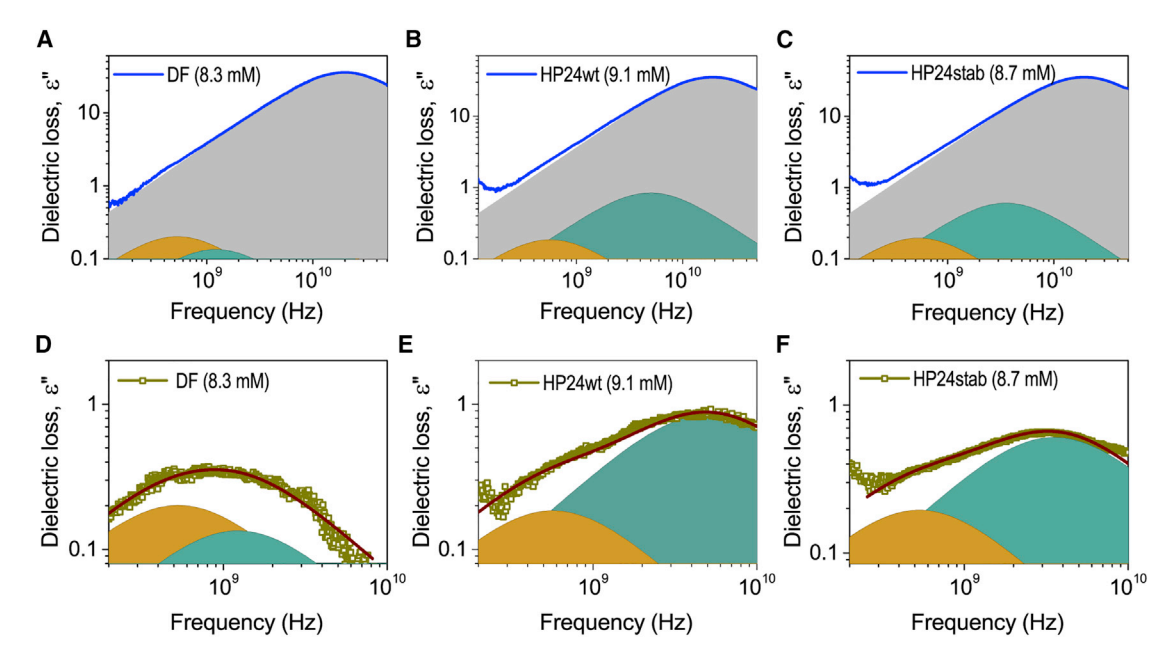


FIGURE 4 Dielectric response of protein solutions is plotted. The dielectric spectra of (A) DF, (B) HP24wt, and (C) HP24stab solutions are deconvoluted into three Debye components, assigning to contributions from TB water (yellow), LB water (green), and bulk water orientational dynamics (gray). The dielectric spectra for protein solvation are shown for (D) DF, (E) HP24wt, and (F) HP24stab, indicating contributions to the dielectric response from hydration water molecules only. To see this figure in color, go online.

in free energy are required for folding (65). Structure formation upon binding yields a less-TB hydration layer. Changes in the hydration layer can also help to offset the entropic cost of binding between IDPs or between IDRs. The IDPs we have studied are all involved in binding. DF and DS are binding domains of, respectively, fibrinogen (66) and stannin (51), and DM is involved in actin binding assemblies with myosin II (67,68). The entropic cost of association of structured proteins is in some cases also offset at least in part by the release of TB water molecules (69–71).

We consider now coupled IDP-water dynamics, revealed both in the dielectric spectra and MD simulation results. A broad dielectric response with a maximum at ≈ 0.3 THz has been observed for all hydrated proteins. The complex dielectric response for the IDP exhibits a peak around 1 THz, which is absent for both HP24wt and HP24stab (Fig. 5). The THz region corresponds to large-scale conformational dynamics of biomolecules (72,73). It is of interest to identify the IDP motions that couple to the water around 1 THz, yielding a peak in the spectrum, which is absent for the solutions with structured proteins. We have computed the VDOS for all five systems and have broken down the contributions into side chains and backbone. These contributions and the full VDOS are plotted for the five systems in Fig. 5. We note that the VDOS does not capture the experimental peak at 0.3 THz. However, we find key differences between the IDPs and structured proteins around 1 THz, as seen in the measured spectra. The VDOS of HP24 is dominated largely by sidechain contributions. On the other hand, there is considerably more contribution of backbone motion to the VDOS for the more flexible IDPs. The emergence of substantial backbone contributions to the VDOS for the IDPs is consistent with dynamic coupling between backbone motions and hydration water dynamics, giving rise to a peak at 1 THz in the complex dielectric response of DF observed in Fig. 5.

Finally, information about the hydration layer that we have determined from the dielectric measurements and the MD simulations, in particular the sizable number of TB water molecules to the surface of IDPs, can provide insights into the mobility of IDPs compared with the mobility of structured proteins of similar size. Different trends are observed, depending on the extent to which the environment of the IDP

TABLE 4 Results from dielectric response spectroscopy

Solutions	$\Delta arepsilon_1$	τ_1 (ps)	$\Delta arepsilon_2$	τ_2 (ps)	$\Delta arepsilon_D$	$\tau_{\mathrm{D}}\left(\mathrm{ps}\right)$	$\sigma (S \cdot m^{-1})$	$N_{ m hyd}$	N _{TBW} (EMA)
Water	_	_	_	_	73.25	8.27 ± 0.20	_	_	_
DF (8.3 mM)	0.30 ± 0.05	305 ± 35	0.20 ± 0.04	131 ± 10	70.46 ± 0.22	8.23 ± 0.20	0.168	200 ± 25	90 ± 10
HP24wt (9.1 mM)	0.37 ± 0.05	280 ± 35	1.68 ± 0.20	32 ± 5	70.07 ± 0.22	8.22 ± 0.20	0.218	218 ± 25	73 ± 8
HP24stab (8.7 mM)	0.39 ± 0.05	310 ± 35	1.22 ± 0.15	45 ± 5	69.49 ± 0.22	8.25 ± 0.20	0.174	272 ± 30	65 ± 8

 $N_{
m hyd}$ is the number of hydration water molecules, $N_{
m TBW}$ is the number of TB water molecules, and σ is the electrical conductivity of the solution. Time constants associated with TB, LB, and bulk water are τ_1 , τ_2 , and τ_D , respectively. The dielectric strength for TB, LB, and bulk water is $\Delta \varepsilon_1$, $\Delta \varepsilon_2$, and $\Delta \varepsilon_D$, respectively.

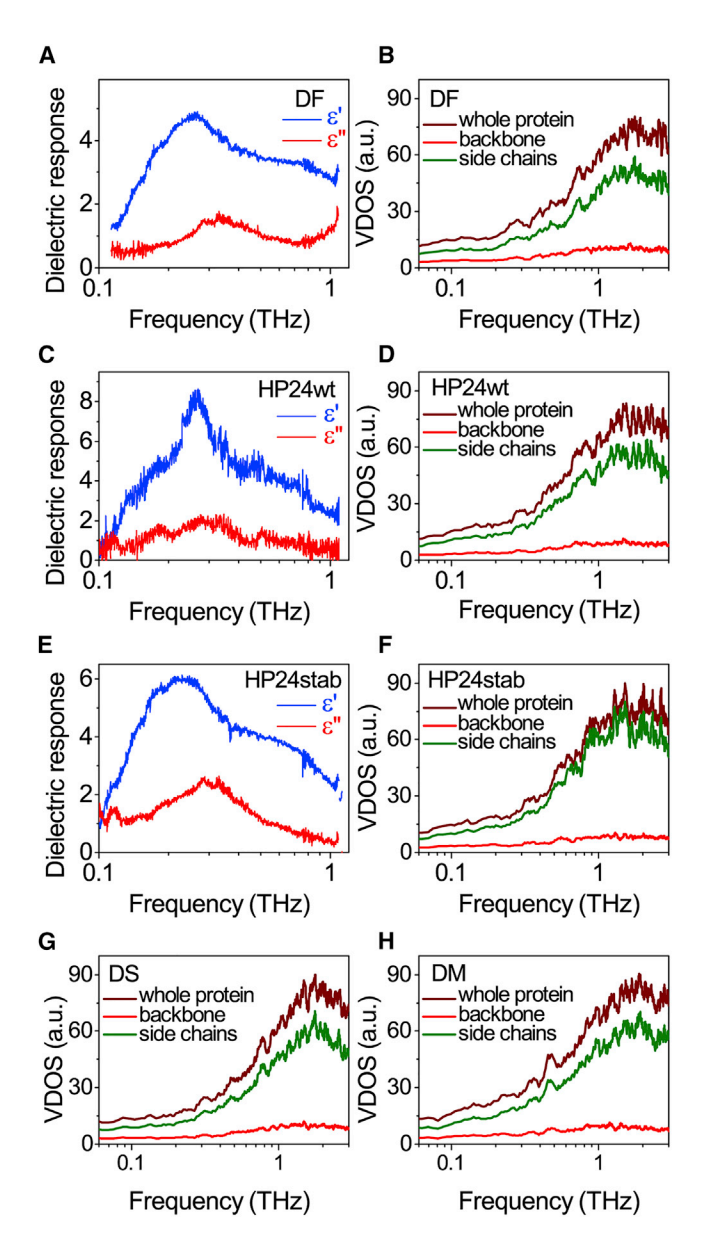


FIGURE 5 Complex dielectric responses corresponding to the collective vibrational motions in hydrated (A) DF, (C) HP24wt, and (E) HP24stab. The VDOS is shown for (B) DF, (D) HP24wt, (F) HP24stab, (G) DS, and (H) DM, computed for backbone, sidechains, and the whole protein. To see this figure in color, go online.

is crowded by other proteins (74–77). In vitro NMR and single-molecule spectroscopy measurements reveal that IDP mobility in dilute solution is slower than the mobility of structured proteins with a similar number of residues (76). The additional TB water molecules to the IDP, found in this work, increases the effective size of the IDP, as we saw when fitting Eq. 8 to the results of the dielectric measurements, consistent with a smaller diffusion coefficient. However, in crowded environments, the mobility of IDPs has been measured to be greater than the mobility of structured proteins of similar size (74–77). In this case, the mobility is influenced less by protein-water interactions and more by protein-protein interactions that result in configurational changes of IDPs in ways that enhance their mobility.

CONCLUSIONS

We have examined the dynamics of IDPs in aqueous solutions by megahertz-to-terahertz dielectric spectroscopy and by MD simulations, including hydration water dynamics, the nature and extent of the hydration layer, and dynamic coupling between IDPs and hydration water. We have compared these properties with those of two more structured systems of similar size. Overall, we find greater heterogeneity in the dynamics of water molecules surrounding IDPs than water surrounding structured proteins. The wider range of relaxation times found for water molecules around both charged and neutral residues of IDPs compared with the corresponding residues of structured proteins yields, on average, more restricted motion of water molecules in the vicinity of IDPs.

The greater number of charged groups of IDPs draws more water molecules closer to them, yielding an excess of TB water molecules to IDPs and the on-average more restricted dynamics. While there are more TB water molecules around IDPs compared with structured proteins of similar size, the size of the hydration layer around IDPs is found to be smaller. This finding is consistent with early models of biological water (37,38) where many water molecules in contact with a protein are TB, exchanging with more LB water in the immediate surroundings, which in turn exchange with bulk water.

We also examined dynamic coupling between the IDPs and water, seen in the dielectric spectra at terahertz frequencies, where a notable enhancement of dynamic coupling is observed compared with the structured systems. The difference, as revealed by the results of the MD simulations, arises from greater IDP backbone-water dynamic coupling compared with structured protein backbone-water coupling.

The adaptability of IDPs in recognition has been attributed to their structural flexibility, which can afford thermodynamic advantages in binding (4). That picture, however, remains incomplete until the role of water around the IDPs is included. Based on the results of our study, we have estimated the decrease in entropy associated with the TB water molecules around IDPs.

SUPPORTING MATERIAL

Supporting material can be found online at https://doi.org/10.1016/j.bpj. 2022.01.011.

AUTHOR CONTRIBUTIONS

K.M.R., N.Q.V., and D.M.L. designed research. N.Q.V., Y.T.-G., and D.M.L. supervised research. K.M.R., A.K.S., and N.Q.V. provided experimental results. K.M.R., J.W., and D.M.L. provided computational results. C.R.B. and Y.T.-G. provided the synthesized samples. K.M.R. and A.K.S. contributed equally to this work. All authors wrote the paper.

ACKNOWLEDGMENTS

We gratefully acknowledge helpful discussions with Prof. Katie Mitchell-Koch, Dr. Jayangika Dahanayake, and Prof. Matthias Heyden. This research was supported by NSF CHE-1854271 (to D.M.L.) and by the National Institutes of Health R35GM128651 (to Y.T.-G.). N.Q.V. and A.K.S. gratefully acknowledge financial support by the Air Force Office of Scientific Research under award number FA9550-18-1-0263 and National Science Foundation (CHE-1665157).

REFERENCES

- Deiana, A., S. Forcelloni, ..., A. Giansanti. 2019. Intrinsically disordered proteins and structured proteins with intrinsically disordered regions have different functional roles in the cell. *PLoS One*. 14:e0217889
- Zosel, F., A. Soranno, ..., B. Schuler. 2020. Depletion interactions modulate the binding between disordered proteins in crowded environments. *Proc. Natl. Acad. Sci. U S A.* 117:13480–13489.
- Chong, S. H., P. Chatterjee, and S. Ham. 2017. Computer simulations of intrinsically disordered proteins. *Annu. Rev. Phys. Chem.* 68:117– 134.
- Tompa, P. 2014. Multisteric regulation by structural disorder in modular signaling proteins: an extension of the concept of allostery. *Chem. Rev.* 114:6715–6732.
- Macossay-Castillo, M., G. Marvelli, ..., S. J. Wodak. 2019. The balancing act of intrinsically disordered proteins: enabling functional diversity while minimizing promiscuity. J. Mol. Biol. 431:1650–1670.
- 6. Motlagh, H. N., J. O. Wrabl, ..., V. J. Hilser. 2014. The ensemble nature of allostery. *Nature*. 508:331–339.
- Bellissent-Funel, M.-C., A. Hassanali, ..., A. E. Garcia. 2016. Water determines the structure and dynamics of proteins. *Chem. Rev.* 116:7673–7697.
- 8. Heyden, M. 2019. Heterogeneity of water structure and dynamics at the protein-water interface. *J. Chem. Phys.* 150:094701.
- Meister, K., S. Ebbinghaus, ..., M. Havenith. 2013. Long-range protein-water dynamics in hyperactive insect antifreeze proteins. *Proc. Natl. Acad. Sci. U S A*. 110:1617–1622.
- Lee, Y., S. Kim, ..., C. Hyeon. 2014. Ultraslow water-mediated transmembrane interactions regulate the activation of A2A adenosine receptor. *Biophys. J.* 111:1180–1191.
- Leitner, D. M., C. Hyeon, and K. M. Reid. 2020. Water-mediated biomolecular dynamics and allostery. J. Chem. Phys. 152:240901.
- Ebbinghaus, S., S. J. Kim, ..., M. Havenith. 2007. An extended dynamical hydration shell around proteins. *Proc. Natl. Acad. Sci. U S A*. 104:20749–20752.
- Leitner, D. M., M. Havenith, and M. Gruebele. 2006. Biomolecule large amplitude motion and solvation dynamics: modeling and probes from THz to X-rays. *Int. Rev. Phys. Chem.* 25:553–582.
- Bagchi, B. 2005. Water dynamics in the hydration layer around proteins and miscelles. *Chem. Rev.* 105:3197–3219.
- Laage, D., T. Elsaesser, and J. T. Hynes. 2017. Water dynamics in the hydration shells of biomolecules. *Chem. Rev.* 117:10694–10725.
- Tobias, D. J., N. Sengupta, and M. Tarek. 2010. Molecular dynamics simulation studies of coupled protein and water dynamics. *In Proteins:* Energy, Heat and Signal Flow. D. M. Leitner and J. E. Straub, eds. Taylor and Francis, pp. 361–386.
- Heyden, M., D. J. Tobias, and D. V. Matyushov. 2012. Terahertz absorption of dilute aqueous solutions. J. Chem. Phys. 137:235103.

- Heyden, M., and D. J. Tobias. 2013. Spatial dependence of protein-water collective hydrogen bond dynamics. *Phys. Rev. Lett.* 111:218101.
- LeBard, D. N., and D. V. Matyushov. 2010. Ferroelectric hydration shells around proteins: electrostatics of the protein-water interface. *J. Phys. Chem. B.* 114:9246–9258.
- 20. Martin, D. R., and D. V. Matyushov. 2015. Dipolar nanodomains in protein hydration shells. *J. Phys. Chem. Lett.* 6:407–412.
- Martin, D. R., and D. V. Matyushov. 2017. Terahertz absorption of lysozyme in solution. J. Chem. Phys. 147:084502.
- Levy, Y., and J. N. Onuchic. 2006. Water mediation in protein folding and molecular recognition. *Annu. Rev. Biophys. Biomol. Struct.* 35:389–415.
- Gavrilov, Y., J. D. Leuchter, and Y. Levy. 2017. On the coupling between the dynamics of protein and water. *Phys. Chem. Chem. Phys.* 19:8243–8257.
- Adams, E. M., S. Pezzotti, ..., M. Havenith. 2021. Local mutations can serve as a game changer for global protein solvent interaction. *JACS Au.* 1:1076–1085.
- Kurisaki, I., C. Barberot, ..., M. Nagaoka. 2015. Dewetting of S1-pocket via water channel upon thrombin-substrate association reaction. *J. Phys. Chem. B*. 119:15807–15812.
- Heyden, M., and M. Havenith. 2010. Combining THz spectroscopy and MD simulations to study protein-hydration coupling. *Methods*. 52:74– 83.
- Persson, F., P. Söderhjelm, and B. Halle. 2018. How proteins modify water dynamics. J. Chem. Phys. 148:215103.
- Dahanayake, J. N., and K. R. Mitchell-Koch. 2018. Entropy connects water structure and dynamics in protein hydration layer. *Phys. Chem. Chem. Phys.* 20:14765–14777.
- Dahanayake, J. N., E. Shahryari, ..., K. R. Mitchell-Koch. 2019. Protein solvent shell structure provides a rapid analysis of hydration dynamics. *J. Chem. Inf. Model.* 59:2407–2422.
- Gallat, F. X., A. Laganowsky, ..., M. Weik. 2012. Dynamical coupling
 of intrinsically disordered proteins and their hydration water: comparison with folded soluble and membrane proteins. *Biophys. J.* 103:129–
 136.
- Arya, S., A. K. Singh, ..., S. Mukhopadhyay. 2018. Femtosecond hydration map of intrinsically disordered alpha-synuclein. *Biophys. J.* 114:2540–2551.
- Chowdhury, A., S. A. Kovalenko, ..., E. A. Lemke. 2019. Mechanism-dependent modulation of ultrafast interfacial water dynamics in intrinsically disordered protein complexes. *Angew. Chem. Int. Ed. Engl.* 58:4720–4724.
- Rani, P., and P. Biswas. 2015. Local structure and dynamics of hydration water in intrinsically disordered proteins. *J. Phys. Chem. B*. 119:10858–10867.
- Aggarwal, L., and P. Biswas. 2018. Hydration water distribution around intrinsically disordered proteins. J. Phys. Chem. B. 122:4206– 4218.
- Rani, P., and P. Biswas. 2015. Diffusion of hydration water around intrinsically disordered proteins. J. Phys. Chem. B. 119:13262–13270.
- Mukhopadhyay, S. 2020. The dynamism of intrinsically disordered proteins: binding-induced folding, amyloid formation, and phase separation. J. Phys. Chem. B. 124:11541–11560.
- Nandi, N., and B. Bagchi. 1997. Dielectric relaxation of biological water. J. Phys. Chem. B. 101:10954–10961.
- Pal, S. K., J. Peon, ..., A. Zewail. 2002. Biological water: femtosecond dynamics of macromolecular hydration. *J. Phys. Chem. B*. 106:12376– 12395.
- Hocking, H. G., F. Hase, ..., G. Zoldak. 2015. A compact native 24-residue supersecondary structure derived from the villin headpiece subdomain. *Biophys. J.* 108:678–686.
- Abraham, M. J., T. Murtola, ..., E. Lindahl. 2015. GROMACS: high performance molecular simulations through multi-level parallelism from laptops to supercomputers. *SoftwareX*. 1–2:19–25.

- 41. Singh, A. K., C. Wen, ..., N. Q. Vinh. 2021. Long-range DNA-water interactions. Biophys. J. 120:4966-4979.
- 42. Charkhesht, A., C. K. Regmi, ..., N. Q. Vinh. 2018. High-precision megahertz-to-terahertz dielectric spectroscopy of protein collective motions and hydration dynamics. J. Phys. Chem. B. 122:6341-6350.
- 43. Nagy, G., M. Igaev, ..., H. Grubmuller. 2019. SESCA: predicting circular dichroism spectra from protein molecular structures. J. Chem. Theory Comput. 15:5087-5102.
- 44. George, D. K., A. Charkhesht, and N. Q. Vinh. 2015. New terahertz dielectric spectroscopy for the study of aqueous solutions. Rev. Sci. Instrum, 86:123105.
- 45. George, D. K., A. Charkhesht, ..., N. Q. Vinh. 2016. New insights into the dynamics of zwitterionic micelles and their hydration waters by gigahertz-to-terahertz dielectric spectroscopy. J. Phys. Chem. B. 120:10757-10767.
- 46. Charkhesht, A., D. Lou, ..., N. Q. Vinh. 2019. Insights into hydration dynamics and cooperative interactions in glycerol-water mixtures by terahertz dielectric spectroscopy. J. Phys. Chem. B. 123:8791–8799.
- 47. Vinh, N. Q., M. S. Sherwin, ..., K. W. Plaxco. 2015. High-precision gigahertz-to-terahertz spectroscopy of aqueous salt solutions as a probe of the femtosecond-to-picosecond dynamics of liquid water. J. Chem. Phys. 142:164502.
- 48. Ellison, W. J. 2007. Permittivity of pure water, at standard atmospheric pressure, over the frequency range 0-25 THz and the temperature range 0-100 degrees C. J. Phys. Chem. Ref. Data. 36:1-18.
- 49. Buchner, R., and G. Hefter. 2009. Interactions and dynamics in electrolyte solutions by dielectric spectroscopy. Phys. Chem. Chem. Phys. 11:8984-8999.
- 50. Böttcher, C. J. F., and P. Bordewijk. 1978. Theory of Electric Polarization, Dielectrics in Time-Dependent Fields. Elsevier Science B. V.
- 51. Buck-Koehntop, B. A., A. Mascioni, ..., G. Veglia. 2005. Structure, dynamics, and membrane topology of stannin: a mediator of neuronal cell apoptosis induced by trimethyltin chloride. J. Mol. Biol. 354:652-665.
- 52. Uversky, V. N. 2011. Intrinsically disordered proteins from A to Z. Int. J. Biochem. Cell Biol. 43:1090-1103.
- 53. Jakob, U., R. Kriwacki, and V. N. Uversky. 2014. Conditionally and transiently disordered proteins: awakening cryptic disorder to regulate protein function. Chem. Rev. 114:6779-6805.
- 54. Cametti, C., S. Marchetti, ..., G. Onori. 2011. Dielectric relaxation spectroscopy of lysozyme aqueous solutions: analysis of the deltadispersion and the contribution of the hydration water. J. Phys. Chem. B. 115:7144-7153.
- 55. Vinh, N. Q., S. J. Allen, and K. W. Plaxco. 2011. Dielectric spectroscopy of proteins as a quantitative experimental test of computational models of their low-frequency harmonic motions. J. Am. Chem. Soc. 133:8942-8947.
- 56. Leitner, D. M., M. Gruebele, and M. Havenith. 2008. Solvation dynamics of biomolecules: modeling and terahertz experiments. HFSP J. 2:314-323.
- 57. Ebbinghaus, S., S. J. Kim, ..., M. Havenith. 2008. Protein sequenceand pH-dependent hydration probed by terahertz spectroscopy. J. Am. Chem. Soc. 130:2374-2375.
- 58. Choy, T. C. 1999. Effective Medium Theory: Principle and Applications. Oxford University Press.

- 59. Bruggemann, D. A. G. 1935. Berechnung verschiedener physikalischer konstanten von heterogenen substanzen. Ann. Phys. 24:636-664.
- 60. Hanai, T. 1960. Theory of the dielectric dispersion due to the interfacial polarization and its application to emulsions. Colloid Polym. Sci.
- 61. Garnett, J. C. M. 1904. Colours in metal glasses and in metallic films. Philos. Trans. R. Soc. A. 203:385-420.
- 62. Ikeda-Saito, M., T. Yonetani, ..., E. Antonini. 1983. Thermodynamic properties of oxygen equilibria of dimeric and tetrameric hemoglobins from Scapharca inaequivalvis. J. Mol. Biol. 170:1009-1018.
- 63. Shammas, S. L., M. D. Crabtree, ..., J. Clarke. 2016. Insights into coupled folding and binding mechanisms from kinetic studies. J. Biol. Chem. 291:6689-6695.
- 64. Tran, D. P., and A. Kitao. 2020. Kinetic selection and relaxation of the intrinsically disordered region of a protein upon binding. J. Chem. Theory Comput. 16:2835-2845.
- 65. Onuchic, J. N., Z. Luthey-Schulten, and P. G. Wolynes. 1997. Theory of protein folding: the energy landscape perspective. Ann. Rev. Phys. Chem 48:545-600
- 66. Yang, Z., J. M. Kollman, ..., R. F. Doolittle. 2001. Crystal structure of native chicken fibrinogen at 2.7 Å resolution. Biochemistry. 40:12515-12523.
- 67. Ronen, D., M. M. Rosenberg, ..., S. Ravid. 2010. The positively charged region of the myosin IIC non-helical tailpiece promotes filament assembly. J. Biol. Chem. 285:7079-7086.
- 68. Betapudi, V. 2014. Life without double-headed non-muscle myosin II motor proteins. Front. Chem. 2:1-13.
- 69. Laine, J. M., M. Amat, ..., F. Massi. 2014. Insight into the allosteric mechanism of Scapharca dimeric hemoglobin. Biochemistry. 53:7199-7210.
- 70. Reid, K. M., X. Yu, and D. M. Leitner. 2021. Change in vibrational entropy with change in protein volume estimated with mode Grüneisen parameters. J. Chem. Phys. 154:055102.
- 71. Ikeda-Saito, M., T. Yonetani, ..., E. Antonini. 1983. Thermodynamic properties of oxygen equilibria of dimeric and tetrameric hemoglobins from Scapharca inaequivalvis. J. Mol. Biol. 170:1009-1018.
- 72. Acbas, G., K. A. Niessen, ..., A. G. Markelz. 2014. Optical measurements of long-range protein vibrations. Nat. Commun. 5:3076.
- 73. Niessen, K. A., M. Xu, ..., A. G. Markelz. 2019. Protein and RNA dynamical fingerprinting. Nat. Commun. 10:1026.
- 74. Soranno, A., I. Köning, ..., B. Schuler. 2014. Single-molecule spectroscopy reveals polymer effects of disordered proteins in crowded environments. Proc. Natl. Acad. Sci. U S A. 111:4874-4879.
- 75. König, I., A. Soranno, ..., B. Schuler. 2021. Impact of in-cell and in-vitro crowding on the conformations and dynamics of an intrinsically disordered protein. Angew. Chem. Int. Ed. Engl. 60:10724–10729.
- 76. Wang, Y., L. A. Benton, ..., G. J. Pielak. 2012. Disordered protein diffusion under crowded conditions. J. Phys. Chem. Lett. 3:2703-2706.
- 77. Lee, J., S. H. Park, ..., J. H. Lee. 2020. High-resolution diffusion measurements of proteins by NMR under near-physiological conditions. Anal. Chem. 92:5073-5081.